Spin phases of the helimagnetic insulator Cu_{2}OSeO_{3} probed by magnon heat conduction

N. Prasai, A. Akopyan, B. A. Trump, G. G. Marcus, S. X. Huang, T. M. McQueen, and J. L.
Cohn

Spin phases of the helimagnetic insulator Cu_2OSeO_3 probed by magnon heat conduction

N. Prasai,[1] A. Akopyan,[1] B. A. Trump,[2, 3, *] G. G. Marcus,[3] S. X. Huang,[1] T. M. McQueen,[2, 3, 4] and J. L. Cohn[1, †]

[1] *Department of Physics, University of Miami, Coral Gables, FL 33124*
[2] *Department of Chemistry, Johns Hopkins University, Baltimore, MD 21218*
[3] *Department of Physics and Astronomy, Institute for Quantum Matter,*
Johns Hopkins University, Baltimore, MD 21218
[4] *Department of Material Science and Engineering,*
Johns Hopkins University, Baltimore, MD 21218

We report studies of thermal conductivity as functions of magnetic field and temperature in the helimagnetic insulator Cu_2OSeO_3 that reveal novel features of the spin-phase transitions as probed by magnon heat conduction. The tilted conical spiral and low-temperature skyrmion phases, recently identified in small-angle neutron scattering studies, are clearly identified by sharp signatures in the magnon thermal conductivity. Magnon scattering associated with the presence of domain boundaries in the tilted conical phase and regions of skyrmion and conical-phase coexistence are identified.

The cubic chiral magnets (MnSi, FeGe, Cu_2OSeO_3) have attracted considerable attention for their complex variety of non-collinear spin phases that include spin modulations with long periods (many lattice spacings) and topological skyrmion phases. Their similar and rich magnetic phase diagrams are dictated by their common noncentrosymmetric cubic lattice symmetry and a hierarchy of competing energy scales (e.g. exchange, Dzyaloshinsky-Moriya, magnetocrystalline anisotropy, Zeeman). Recently two new spin phases, low-temperature skyrmion and "titled conical spiral," were identified in the insulating compound Cu_2OSeO_3 by small-angle neutron scattering (SANS) [1, 2]. These novel phases, arising at low temperature and relatively high magnetic field, reflect competing Zeeman and anisotropy energies that lead to surprising spin textures and a re-orientation of the long-period spin modulation direction.

Here we report that field dependent thermal conductivity measurements are a particularly sensitive probe of the spin phase transitions in Cu_2OSeO_3 because of the compound's unprecedentedly large magnon heat conductivity [3]. Rather little is known experimentally about magnons in ferro- or ferri-magnets from heat transport, their scattering or its dependency on spin textures, whether long-range ordered or not. Such information has increased in its importance and relevance with the surging interest in spintronic and magnonic device applications [4, 5]. Cu_2OSeO_3 is an ideal material for investigating these characteristics because the spin and lattice systems are weakly coupled as evidenced by very low spin-lattice damping [6, 7] and by mean-free paths for both magnons and phonons as large as 0.3 mm below 2K [3]. These conditions ensure that energy (e.g. from a heater in thermal conductivity measurements) is transferred from the lattice to the spin system, but is weak enough so the contributions from phonons (κ_L) and magnons (κ_m) are approximately additive [3, 8], $\kappa \simeq \kappa_L + \kappa_m$.

Our measurements reveal a complete suppression of the magnon heat flux in the tilted conical phase along the $\langle 110 \rangle$ directions that we attribute to strong magnon scattering by tilt domain boundaries. This observation raises the prospect of exploiting this configuration of heat flux and applied field in a field-controllable spin-current switch. The low-temperature skyrmion phase, characterized by long-range skyrmion lattice order, supports maximum magnon heat conduction comparable to that of the fully polarized phase. Suppressed magnon heat conduction characterizes regions of phase coexistence.

Cu_2OSeO_3 comprises a three-dimensional distorted pyrochlore (approximately fcc) lattice of corner-sharing Cu tetrahedra [9, 10]. Strong magnetic interactions within tetrahedra lead to a 3-up-1-down, spin $S = 1$ magnetic state [11, 12] with weaker interactions between tetrahedra leading to their ferromagnetic ordering below $T_C \simeq 58$ K. At low temperatures [13, 14] the low-field state is helimagnetic wherein the atomic spins rotate within a plane perpendicular to the helical axis with a wavelength $\lambda_h \simeq 62$ nm; multiple domains with helices aligned along $\langle 100 \rangle$ directions (easy axes) characterize this phase. At $H \gtrsim 10 - 25$ mT (depending on field orientation) the helices of individual domains rotate along the field to form a single-domain, conical phase in which spins rotate on the surface of a cone. Further increasing the field narrows the conical angle until $H \gtrsim 50 - 75$ mT where the ferrimagnetic, fully-polarized (collinear) state emerges. Until recently, these three phases comprised a universal phase diagram for the cubic chiral magnets.

Our prior studies of this compound for heat flow along [111] [*cf.* Fig. 3 (e)] demonstrate that the field dependent changes in κ are entirely magnonic. A separation of κ_L and κ_m is possible at high fields since spin-wave excitations are gradually depopulated (gapped) with increasing field following the Zeeman energy $E_H = g\mu_B H$, and are completely suppressed for $E_H \gg k_B T$ where $\kappa \to \kappa_L$ [15–22]. This decomposition, at $T \lesssim 1.2$ K where the high-field condition applies, is discussed in detail for [111]-oriented specimens in Ref. 3. That work demonstrates mean-free paths for both phonons and magnons comparable to the transverse specimen dimensions at $T \lesssim 2$ K
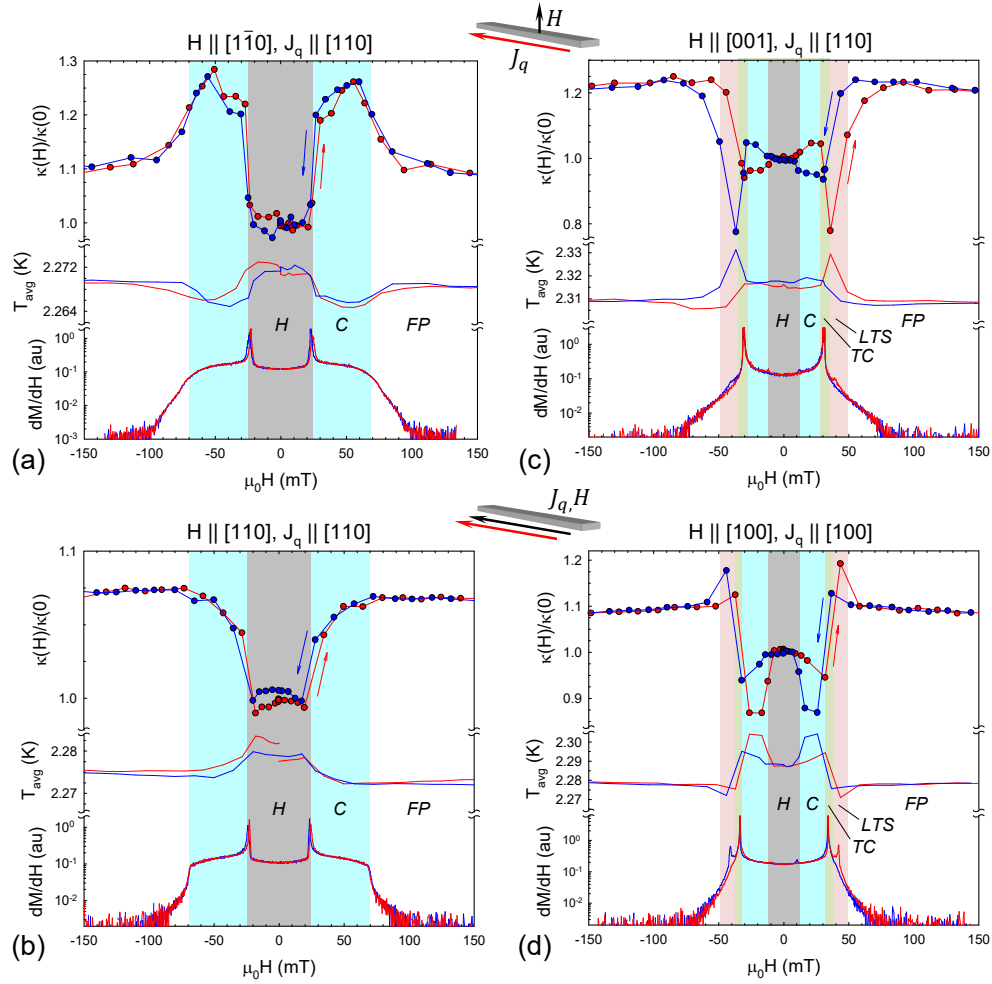
FIG. 1. (a)-(d): κ, T_{avg} and dM/dH vs field (corrected for demagnetization) at $T \simeq 2.30$ K for four configurations of the applied field and heat flow. $H \perp J_q$ for (a) and (c), $H||J_q$ for (b) and (d). Specimens were cooled in zero field and hysteresis loops traversed sequentially from (arrows, upper panel): $\mu_0 H = 0 \to 200$ mT, 200 mT $\to -200$ mT, -200 mT $\to 0$. The spin phases are distinguished by different background shading and labels: helical (H), conical (C), tilted conical (TC), low-temperature skyrmion (LTS), and fully polarized (FP).

and maximum values for $\kappa_m \sim 20-80$ W/mK, the largest known for ferro- or ferri- magnets. Values for κ_L and κ_m vary modestly between specimens due to size effects and a small and variable Se vacancy concentration [3].

Phase pure, single crystals of Cu_2OSeO_3 were grown by chemical vapor transport as described previously [23]. Specimens were cut from single-crystal ingots, oriented by x-ray diffraction, and polished into thin parallelopipeds. A two-thermometer, one-heater method was employed to measure the thermal conductivity in applied magnetic fields up to 50 kOe. Specimens were suspended from a Cu heat sink with silver epoxy and affixed with a 1 kΩ chip heater on the free end. A matched pair of RuO bare-chip sensors, calibrated in separate experiments and mounted on thin Cu plates, were attached to the specimen through 5 mil. diameter Au-wire thermal links bonded to the Cu plates and specimen with silver epoxy. Measurements were performed in a ^{3}He "dipper"

probe with integrated superconducting solenoid. Magnetization measurements were performed in separate experiments using a Quantum Design PPMS system. The dimensions, orientations, and demagnetization factors of all specimens can be found in the Supplemental Material [24].

Figure 1 (a)-(d) show the field dependent (normalized) thermal conductivities, $\kappa(H)/\kappa(0)$, and average specimen temperatures, T_{avg} (upper and middle panels, respectively) for four different configurations of the applied field (H) and heat flow (J_q): $H \perp J_q$ for (a), (c) and $H||J_q$ for (b), (d). The derivative of the magnetization, dM/dH (lower panels), was determined from separate measurements on the same specimens (all field values represent internal fields, corrected for demagnetization [25]). The background shading distinguishes the spin phases. Three spin phases, helical (H), conical (C), and fully polarized (FP), are clearly reflected in the three
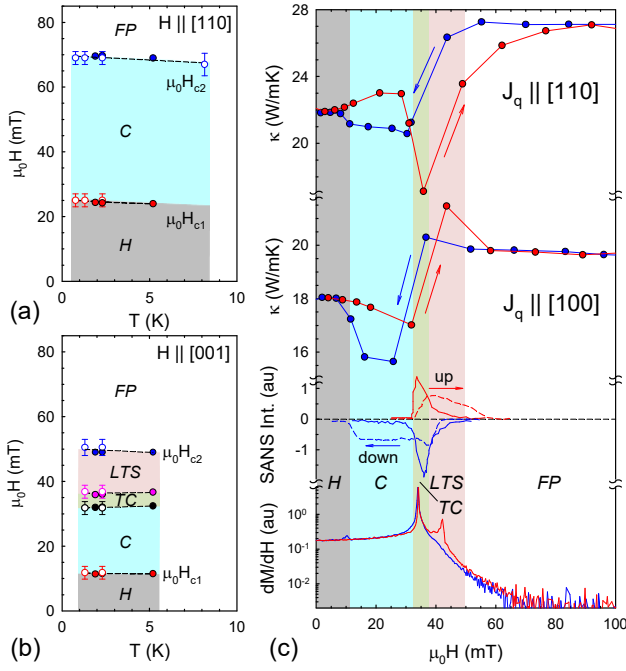
FIG. 2. Low-T phase diagrams for (a) $H||[110]$ and (b) $H||[001]$. Filled (open) points are from features in dM/dH (κ). Dashed lines are guides. (c) Upper panels: the $H > 0$ portion of $\kappa(H)$ scans from Fig. 1 (c) and (d). Middle panel: SANS intensities for increasing ("up") and decreasing ("down") fields (from Ref. 26) for the TC (solid curves) and LTS (dashed curves) phases. Field values for the SANS data were shifted upward by 5 mT to align the onset of the TC-phase intensity with the leading edge of the sharp peak in dM/dH, consistent with the calibration established in Ref. 26. Lower panel: dM/dH from Fig. 1 (d).

measured quantities for $H||\langle 110\rangle$ [Fig. 1 (a), (b)]. Note that the average specimen temperature is stable to within 3-4 mK during measurements (conducted at a series of stabilized field values). Abrupt changes in T_{avg} at the spin-phase transitions mirror those in κ and reflect energy exchange between the spin system and lattice under the near-adiabatic conditions of the measurements [3].

Additional sharp features and strong hysteresis distinguish the field-dependent quantities for $H||\langle 100\rangle$ [Fig. 1 (c), (d)] from those with $H||\langle 110\rangle$. These additional features are attributed to the tilted conical (TC) and low-temperature skyrmion (LTS) phases, identified in SANS [1, 2] as unique to the $H||\langle 100\rangle$ orientation. Phase diagrams are plotted in Fig. 2 based on features observed in the field dependencies of κ and dM/dH; for the latter we followed the calibration of dM/dH against SANS established by Halder *et al.* [26], discussed in more detail below. Changes in $\kappa(H)$ upon traversing the various phase boundaries are the principal results and focus of this work.

For $H||\langle 110\rangle$ [Fig.'s 1 (a), (b)], we see that κ increases sharply with increasing field upon crossing the helical-conical phase boundary. This clearly reflects the elimi-

nation of domain boundary scattering of magnons as the multidomain helical phase, with three mutually perpendicular spiral spin domains aligned along the $\langle 100\rangle$ directions, is converted to a single domain with conical spiral axis along the applied field. Note that this step-like enhancement of κ occurs in Fig.'s 1 (a) and (b) regardless of the conical spiral direction transverse to or along the heat flow. Within the conical phase κ increases as the conical angle decreases, and for $H||[1\bar{1}0]$ abruptly *decreases* upon entering the fully polarized state [Fig. 1 (a)]. A similar behavior was observed for the same field orientation with [111] heat flow [3]. Though a larger intrinsic spin gap in the fully polarized state might explain these features, the specific heat shows only a modest, $\lesssim 5$ % decline through the C-FP transition [26], suggesting a more substantial decline in the magnon mean-free path.

The more complex and hysteretic behaviors for $\kappa(H)$ with $H||\langle 100\rangle$ are correlated in Fig. 2 (c) against the SANS [26] and magnetization data through a more detailed comparison of the positive field portions of Fig.'s 1 (c) and (d); the SANS intensities for the TC and LTS phases for both ascending ("up") and descending ("down") field are reproduced in the middle panel. The principle features of $\kappa(H)$ are: (1) in ascending field κ increases gradually by ~ 1 W/mK upon entering the conical phase for $J_q||[110]$, but decreases by the same amount for $J_q||[100]$, (2) κ sharply decreases in ascending field upon entering the tilted conical phase for $J_q||[110]$, but increases sharply for $J_q||[100]$, (3) for both orientations κ is maximal or approaches its maximum value in the LTS phase, (4) in descending field for both orientations, the conical phase κ is lower than in ascending field and exhibits a step-like increase toward the zero-field value upon crossing the C-H phase boundary.

Hysteresis, in all of the measured quantities in Fig. 2 (c), has its origin in the strongly first-order character of the transition to the LTS state which involves a large energy barrier requiring the creation of pairs of Bloch points (magnetic monopoles) and is topologically protected [27, 28]. The LTS phase is preceded in both ascending and descending field by the TC phase, but the LTS phase persists to higher and lower fields, respectively. As a result, the LTS phase coexists with the conical phase in descending field and disappears only at the C-H transition (evidenced by the small peak in dM/dH). Clearly the long-range ordered skyrmion spin textures [Fig. 3 (a)] present minimal scattering for magnons [feature (3) above] and thus suppressed values for κ in the conical phase for descending field [feature (4)] are attributed to spin disorder associated with phase coexistence. Feature (1) might be related to channeling of spin waves with momenta transverse to the conical spiral axis [29, 30], but this possibility requires further investigation.

We focus the remainder of our discussion on the sharp drop in κ upon entering the tilted conical phase for $J_q||[110]$ [feature (2)], interpreted to indicate that boundaries between tilted conical domains are extremely effective scatterers of magnons. The domain structure within
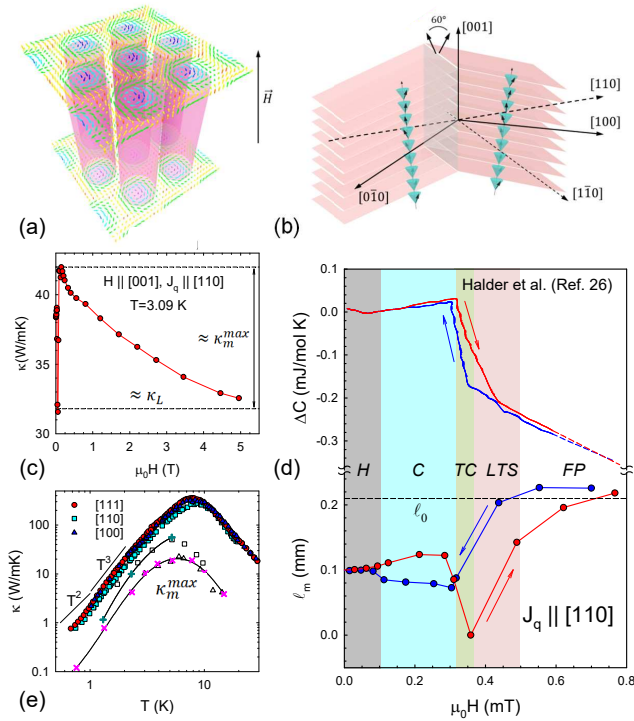
FIG. 3. (a) skyrmion spin textures in the *LTS* phase, (b) an idealized planar boundary between tilted conical domains of the *TC* phase (the planes represent layers of atomic spins oriented in the direction dictated by the adjacent conical spirals), (c) $\kappa(H)$ at $T = 3.09$ K for a second specimen with the same configuration as in Fig. 1 (c), but at higher field in the fully polarized state where $\kappa \to \kappa_L$ due to the field-induced spin gap. Low-field data at additional temperatures for this specimen are presented in Fig. S3 [24], (d) Change with field in the specific heat (from Ref. 26) extended to higher field (dashed lines) and magnon mean-free path computed from kinetic theory as described in the text from data in Fig. 2 (c). The horizontal dashed line indicates the specimen transverse dimension ℓ_0. (e) zero-field $\kappa(T)$ for heat flow along different crystallographic directions. Also shown ($+$, $\times$ and solid curves as guides) are the maximum magnon contributions, κ_m^{max}, inferred for two [110] specimens as described in the text, and for two [111] specimens from Ref. 3 (open squares and triangles).

the *TC* phase has not been established, but since the conical spiral axes tilt away from the [001] field direction toward $\langle 111 \rangle$ directions (by angle $\phi \approx 30°$ at $T = 2$ K [1, 2]), a planar boundary transverse to the heat flow, as depicted in Fig. 3 (b) for two such domains, is possible. Even for a boundary with a more realistic transition region of finite extent, the cross-sectional area of the domain boundary for $H||J_q||[100]$ would be substantially smaller, offering an explanation for the absence of a downturn in κ for this orientation. As noted in Ref. 2, the very small free energy difference for conical spiral alignment along the $\langle 100 \rangle$ and $\langle 111 \rangle$ directions could lead to the formation of a superstructure with a smooth rotation between tilted conical domains. Our results clearly fa-

vor a domain structure that results in highly anisotropic magnon scattering, with strong scattering for magnon momentum *transverse* to the applied field.

Data at higher field (up to 5 T) for a second [110] specimen [Fig. 3 (c)] demonstrate that κ_m is entirely suppressed in the tilted conical phase for this orientation, since $\kappa(5 \text{ T}) \to \kappa_L$ is comparable to the value of κ at the sharp drop upon entering the *TC* phase. Further corroborating this interpretation, the computed magnon mean-free path ℓ_m for $J_q||[110]$ using data of Fig. 2 (c) achieves a maximum value [Fig. 3 (d)] in good agreement with the effective transverse dimension of the sample. Also shown in Fig. 3 (d) are changes in the specific heat with field $\Delta C(H)$ reported in Ref. 26. We used kinetic theory, $\ell_m = 3\kappa_m/(C_m v_m)$, where κ_m was computed from the data assuming $\kappa = \kappa_L$ at the minimum, v_m is the magnon velocity, and $C_m(H)$ was computed from $\Delta C(H)$ (converted to volume units using 1 mol=5.35×10^{-5}m^3) and assuming a magnetic specific heat per volume from, $C_m(0) = (0.113/4)k_B(k_B T/D)^{3/2}$ with spin-wave stiffness $D = 52.6$ meV Å^2 [31]. The dominant magnons for boundary-limited κ_m have $q_{dom} = (2.58 k_B T/D)^{1/2}$ such that $v_m \simeq 1040 T^{1/2}$ m/s [3].

Curves for $\kappa_m^{max}(T)$, determined from the difference between the minimum value and the maximum in the *FP* state, are shown in Fig. 3 (e) ($+$, $\times$ and solid curves) for both [110] specimens [24]; their magnitudes and temperature dependencies, with peaks at $T \approx 5 - 6$ K, are consistent with prior results [3] on $\kappa_m^{max}(T)$ for [111]-oriented specimens with $H||[1\bar{1}0]$ (open squares and triangles). The rapid decline in κ_m^{max} at $T \gtrsim 6$ K for both the [110] and [111] oriented specimens is the signature of other strong, intrinsic magnon scattering (e.g. magnon-magnon Umklapp or magnon-phonon).

That a magnon heat conductivity as large as $\kappa_m^{max} \approx$ 60 W/mK at 5 K [Fig. 3 (e) and Fig. S2 (b) [24]] can be suppressed to zero with a small change in applied field constitutes a novel, insulating spin-current switch [32] that could be exploited to control voltage readout in an interfacial heavy-metal thin film via the inverse spin-Hall effect. Since the tilted conical phase arises from a competition between magnetic anisotropies generic to chiral magnets [1, 2], similar phenomena might be found in other materials and temperature regimes.

In summary, the unprecedentedly large magnon thermal conductivity in Cu$_2$OSeO$_3$ provides a sensitive probe of the transitions in applied field between its spin phases in the ground state. Our survey of various orientations of the heat flow and applied field provide new insight into magnon transport within non-collinear spin phases, the influence of domain interfaces and phase coexistence on magnon scattering, and reveal a new mechanism by which spin currents in insulators may be manipulated.

* Current address: NIST Center for Neutron Research, National Institute of Standards and Technology, Gaithersburg, Maryland 20899-6102

† Corresponding Author: cohn@physics.miami.edu

[1] A. Chacon , L. Heinen, M. Halder, A. Bauer, W. Simeth, S. Mühlbauer, H. Berger, M. Garst, A. Rosch and C. Pfleiderer, Nature Phys. **14**, 936 (2018).

[2] Fengjiao Qian, Lars J. Bannenberg, Heribert Wilhelm, Grégory Chaboussant, Lisa M. Debeer-Schmitt, Marcus P. Schmidt, Aisha Aqeel, Thomas T. M. Palstra, Ekkes Brück, Anton J. E. Lefering, Catherine Pappas, Maxim Mostovoy, and Andrey O. Leonov, Sci. Adv. **4**, 7323 (2018).

[3] N. Prasai, B. A. Trump, G. G. Marcus, A. Akopyan, S. X. Huang, T. M. McQueen, and J. L. Cohn, Phys. Rev. B **95**, 224407 (2017).

[4] Stephen R. Boona, Roberto C. Myers and Joseph P. Heremans, Energy Environ. Sci. **7**, 885 (2014).

[5] A. V. Chumak, V. I. Vasyuchka, A. A. Serga, and B. Hillebrands, Nature Phys. **11**, 453 (2015).

[6] S. Seki et al. Phys. Rev. B **93**, 235131 (2016).

[7] I. Stasinopoulos, S. Weichselbaumer, A. Bauer, J. Waizner, H. Berger, S. Maendl, M. Garst, C. Pfleiderer, and D. Grundler, Appl. Phys. Lett. **111**, 032408 (2017).

[8] D. J. Sanders and D. Walton, Phys. Rev. B **15**, 1489 (1977).

[9] P. G. Meunier and M. Bertaud, J. Appl. Crystallogr. **9**, 364 (1976).

[10] H. Effenberger and F. Pertlik, Monatshefte für Chemie **117**, 887 (1986).

[11] Jan-Willem G. Bos, C. V. Colin, and T. T. M. Palstra, Phys. Rev. B **78**, 094416 (2008).

[12] M. Belesi, I. Rousochatzakis, H. C. Wu, H. Berger, I. V. Shvets, F. Mila, and J. P. Ansermet, Phys. Rev. B **82**, 094422 (2010).

[13] S. Seki, X. Z. Yu, S. Ishiwata, and Y. Tokura, Science **336**, 198 (2012).

[14] T. Adams, A. Chacon, M. Wagner, A. Bauer, G. Brandl, B. Pedersen,H. Berger, P. Lemmens, and C. Pfleiderer, Phys. Rev. Lett. **108**, 237204 (2012).

[15] D. Douthett and S. A. Friedberg, Phys. Rev. **121**, 1662 (1961).

[16] D. C. Mccollum, R. L. Wild and J. Callaway, Phys. Rev. **136**, A426 (1964).

[17] B. Luthi, J. Phys. Chem. Solids **23**, 35 (1962).

[18] R. L. Douglass, Phys. Rev. **129**, 1132 (1963).

[19] C. M. Bhandari and G. S. Verma, Phys. Rev. **152**, 731 (1966).

[20] D. Walton, J. E. Rives, and Q. Khalid, Phys. Rev. B **8**, 1210 (1973).

[21] B. Y. Pan, T. Y. Guan, X. C. Hong, S. Y. Zhou, X. Qiu, H. Zhang, and S. Y. Li, Europhys. Lett. **103**, 37005 (2013).

[22] S. R. Boona and J. P. Heremans, Phys. Rev. B **90**, 064421 (2014).

[23] J. Panella, B. A. Trump, G. G. Marcus, and T. M. McQueen, Cryst. Growth Des. **17**, 4944 (2017).

[24] For additional specimen details and data, see Supplementary Material at http://link.aps.org/supplemental/xx.xxxx/PhysRevB.9x.xxxxxx, which includes Table S1 and Fig.s S1-S3.

[25] Amikam Aharoni, J. Appl. Phys. **83** 3432 (1998).

[26] M. Halder, A. Chacon, A. Bauer, W. Simeth, S. Mühlbauer, H. Berger, L. Heinen, M. Garst, A. Rosch, and C. Pfleiderer, Phys. Rev. B **98**, 144429 (2018).

[27] P. Milde, D. Köhler, J. Seidel, L. M. Eng, A. Bauer, A. Chacon, J. Kindervater, S. Mühlbauer, C. Pfleiderer, S. Buhrandt, C. Schütte, and A. Rosch, Science **340**, 1076 (2013).

[28] J. Wild, T. N. G. Meier, S. Poellath, M. Kronseder, A. Bauer, A. Chacon, M. Halder, M. Schowalter, A. Rosenauer, J. Zweck, J. Müller, A. Rosch, C. Pfleiderer, and C. H. Back, Sci. Adv. **3**, 1701704 (2017).

[29] M. Janoschek, F. Bernlochner, S. Dunsiger, C. Pfleiderer, and P. Böni, B. Roessli, P. Link and A. Rosch, Phys. Rev. B **81**, 214436 (2010).

[30] Markus Garst, Johannes Waizner and Dirk Grundler, J. Phys. D: Appl. Phys. **50** (2017).

[31] P. Y. Portnichenko, J. Romhànyi, Y. A. Onykiienko, A. Henschel, M. Schmidt, A. S. Cameron, M. A. Surmach, J. A. Lim, J. T. Park, A. Schneidewind, D. L. Abernathy, H. Rosner, Jeroen van den Brink and D. S. Inosov, Nat. Commun. **7**, 10725 (2016).

[32] Zhiyong Qiu, Dazhi Hou, Joseph Barker, Kei Yamamoto, Olena Gomonay and Eiji Saitoh, Nature Mater. **17**, 577 (2018).